Journal of Constructional Steel Research 223 (2024) 109034

Contents lists available at ScienceDirect

Journal of Constructional Steel Research

journal homepage: www.elsevier.com/locate/jcsr

Estimation of backbone model parameters for simulation of exposed column base plates

Sergio Villar-Salinas [a,*], Amit Kanvinde [b], Francisco López-Almansa [c]

[a] Civil and Environmental Engineering Department, Universidad Tecnológica de Bolívar, Campus Tecnológico km 1 Vía Turbaco, 130011, Cartagena, de Indias, Colombia
[b] Dept. of Civil and Environmental Engineering, Univ. of California, CA 95616 Davis, USA
[c] Dept. of Architecture Structures, Polytechnic University of Catalonia, Campus Nord UPC, 08034, Barcelona, Spain

ARTICLE INFO

Keywords:
Exposed-column-baseplates
Moment-rotation curves
Axial compression ratio
Regression models
Performance-based assessment

ABSTRACT

An approach is presented for the estimation of the parameters required to simulate the nonlinear monotonic (i.e., backbone) rotational response of Exposed-Column-Base-Plate (ECBP) connections subjected to moment and axial compression. A trilinear backbone curve is selected to represent the rotational response, defined by three deformation and two strength parameters; these properly represent the stiffness, strength, and ductility of the connections. This approach is accompanied by a tool to facilitate convenient estimation of the parameters. The approach is based on a combination of behavioral insights and physics-based models (for some parameters) as well as regression for other parameters, which are estimated from a dataset of eighty-four experiments on ECBP connections conducted over the last forty years in the United States, Europe, and Asia. Predictive equations are provided to estimate the various parameters defining the nonlinear response, and their efficacy is examined by comparing them with the test data; in addition, well-established techniques are implemented to avoid collinearity and the overfitting of regression models. The results show that the models presented in this work provide robust and accurate predictions for in-sample and out-of-sample data. Limitations are outlined.

1. Introduction and motivation

Exposed Column-Base Plate (ECBP) connections are critical components in steel Moment Resisting Frames (MRFs) in seismic regions, transferring all the loads to the foundation and influencing the overall performance of these structures, as noted in numerous studies [1–8]. Despite major advances in the understanding of their strength (e.g., axial, rotational, and shear) and rotational stiffness, important knowledge gaps remain. As noted by Zareian and Kanvinde [9], and Latour and Rizzano [10], there is a significant gap in the guidance area for simulating the nonlinear rotational behavior of these connections within the context of modern performance assessment frameworks. This behavior is complex and a function of the interaction of its components (e.g., column, anchor rods, plate, and concrete), loads, and soil structure interaction, as described by Kanvinde et al. [11]. When base connections are designed to remain elastic, which is common in non-seismic conditions (AISC Desing Guide 1 [12]), and in many seismic conditions as well (AISC 341–22, D2.6c [13]), the primary concern is representing their rotational flexibility (or initial stiffness). Previous studies (e.g., Kanvinde et al. [14] and Latour et al. [15]) have developed models for the estimation of such flexibility. These models have been validated at a laboratory scale (e.g., Gómez et al. [16]), as well as through data obtained from instrumented buildings (Falborski et al. [17]), and indicate that: (i) assuming that the base connection is either fixed or pinned, as is often done, is erroneous, and (ii) base connection configuration has a strong influence on connection rotational stiffness. More recently, there has been a focus on "weak-base" connections in seismic conditions, wherein the base connection is designed to be weaker than the column. Such connections are explicitly mentioned in American design codes, wherein the ECBP may typically be designed for a building base shear corresponding to the overstrength (i.e., the Ω_0- factor, AISC 341–22 [13]). Specifically, studies by Hassan et al. [18], Falborski et al. [17], as well as Trautner et al. [19], indicate that substantial economies may be achieved in connection design if adequate deformation capacity is provided in these connections. However, the implied nonlinear response of these connections (either by design or through unanticipated overloads) necessitates approaches for estimating the full nonlinear response (beyond just the initial rotational stiffness) for performance assessment of structures utilizing weak-bases. Developing such approaches is the primary objective of this paper.

A literature review over the last three decades indicates significant

* Corresponding author.
E-mail address: svillars@utb.edu.co (S. Villar-Salinas).

https://doi.org/10.1016/j.jcsr.2024.109034
Received 3 July 2024; Received in revised form 11 September 2024; Accepted 12 September 2024
0143-974X/© 2024 The Authors. Published by Elsevier Ltd. This is an open access article under the CC BY-NC license (http://creativecommons.org/licenses/by-nc/4.0/).

Notation

ACR	Axial Compression Ratio
A, A_1, A_2	Cross-sectional area of the column, plate bearing area, effective concrete area
A_{rod}, A_p^s	Sectional area of a bolt group in tension, shear area of the plate
b_{eff}, l_{eff}	Effective width and length of a T-Stub (according to Eurocode philosophy)
b_{fc}, t_{fc}	Width, and thickness of the column flanges
B, N	Width and length of the steel plate
B_0, L_0	Distance between bolts along the weak and strong direction of the column
C	Constant used in proposed regression-based equations
CV	Cross Validation for out-of-sample prediction
d, d_{foot}, D_b	Height of the column section and concrete footing, diameter of anchor rods
ECBP	Exposed Column Base Plate
E_b, E_{col}, $E_{concrete}$, E_p	Modulus of elasticity of the bolts, column, concrete, and plate
f	Distance from the centroid of the bolts in tension to the centroid of the column
f'_c, f_{max}	Concrete compressive strength, surface pressure for large eccentricity loading scenario ($= \phi_b\ 0.85\ f'_c$)
F_{yb}, F_{yc}, F_{yp}	Yield stress of bolts, column, and plate
g, G_p	Edge distance, shear modulus of the plate
HSS	Hollow Structural Sections
I_{col}, I_p	Moment of inertia of the column, and plate
k	Number of folds for cross-validation process
K_0^{bp}	Initial rotational stiffnesses of ECBP
K_1^{bp}, θ_1^{bp}	Pre-capping stiffness and rotational parameter for the start of the plastic plateau
L_{col},	Length of the column
m	Cantilever distance of the plate
M-θ	Moment-rotation relationship for ECBP
M_u, P_u, and V_u	Acting moment, axial, and shear loads on the ECBP
M_y^{bp}, M_{max}^{bp}, M_n^{bp}	Yield, ultimate, and predicted (nominal) strengths of the ECBP
M_y^{col}, M_{yp}, M_{yb}	Yield strength of the column, plate, and bolts
$M_{yp}^{tension}$	Yield strength of the plate due to tension force in anchors
$M_{yp}^{comp\text{-}small}$, $M_{yp}^{comp\text{-}large}$	Yield strength of the plate due to bearing pressure on the compression side for small and large eccentricity
OTD	Out-of-trend data
r	Pearson's correlation coefficient
P-M	Axial load-moment
q_{max}	Line-force on the foundation for a large eccentricity condition ($= B\ f_{max}$).
$RMSE$	Root of the mean square errors
R^2	Correlation coefficient
S_f, S_w	Widths of the fillet welds of the flange and web of the column
t_g, t_n, t_p, t_w	Thicknesses of the grout pad, nuts, steel plate, and washers
t, T	Coefficient of t-student test, tensile force in anchor rods
T_{yb}	Yield tensile force of the anchors
$Y1$, $Y2_p$, $Y2_b$	Bearing lengths corresponding to small and large eccentricity (with yielding plate and bolts)
β_0 to β_9	Regression coefficients for the proposed predictive equations
Δ^{col}, $\Delta^{cantiliver}$	Horizontal displacement at the top due to the column and measured horizontal displacement, respectively
ϕ_b	Resistance factor for combined moment and axial force ($= 0.75$)
θ_y^{bp}, θ_{max}^{bp}	Yield and maximum rotations of the ECBP
θ^{bp}	Rotation of ECBP

progress in understanding the ECBP response and developing models to represent it. Studies by Picard and Beaulieu [20], Melchers [21], Hon and Melchers [22], Jaspart and Vandegans [3], and Kavoura and co-workers (refer to [23–25]) collectively indicate that the rotational stiffness of ECBP connections increases with axial load on the column; thus, this stiffness should be considered in the structural analysis. Following this observation, analytical models have been proposed to represent various parts of the load-deformation response. Primarily, these models focus on the strength or stiffness of these connections. For strength characterization, notable work includes that of Salmon et al. [26], Ermopoulos and Stamatopoulos [27], Drake and Elkin [28] (which forms the basis of AISC Design Guide 1 [12]), and Kanvinde et al. [29]. For rotational stiffness characterization, notable work includes Kanvinde et al. [14], Dumas et al. [30], and Diaz et al. [31]. Cumulatively, these models provide reliable ways of characterizing the strength and stiffness of these connections. The former (i.e., the strength) is important from a design perspective, and the latter (i.e., the stiffness) is important from the perspective of representing these connections in linear analysis (or when the base is expected to remain elastic). However, strength and stiffness alone are insufficient for representing the full nonlinear rotational response of these connections, which includes other features corresponding to strain hardening, ductility, and the loss of stiffness as failure modes are initiated. As discussed above, the representation of such a response becomes important when base connections are anticipated to deform into the inelastic range, either by design or unanticipated overloads. In this regard, it is relevant to mention models for estimating the in-cycle ductility (e.g., Latour and Rizzano [32]) and cyclic degradation of ECBP (i.e., Torres-Rodas et al. [33] and Latour and Rizzano [10]). Other than these limited studies (which focus on very specific connection configurations), there is very limited guidance for simulating this full response. Motivated by this, the main objective of this paper is to provide an approach to estimate the parameters defining the full rotational response of ECBP connections. This approach focuses on monotonic response (i.e., the backbone curve) and is based on a combination of mechanistic models (for some parameters) and regression-based predictive equations for others, where the mechanics is not evident. A complimentary web-based tool and database (https://cbp-db-modelling.utb.edu.co/model) of test results is also provided to facilitate convenient and transparent estimation of parameters.

The next section of the paper provides relevant background information, followed by a description of the test database from which the approach is developed. The approach, involving estimation methods for each relevant parameter avoiding collinearity, is then presented and examined against available test data; for regression-based models, reliable techniques are applied to avoid collinearity (i.e., the correlation matrix of predictor variables) and overfitting (e.g., k-fold Cross-Validation CV process). The paper concludes by summarizing the work while also outlining its limitations.

2. Background: A trilinear model for the moment-rotation curves of ECBP

Fig. 1 illustrates a typical ECBP detail common to construction practice in the United States and the general response of this type of

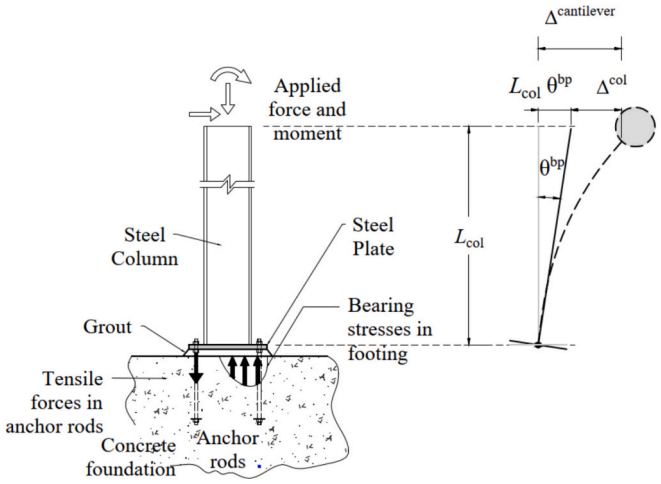

Fig. 1. Typical assembly and general response of ECBP (schematic).

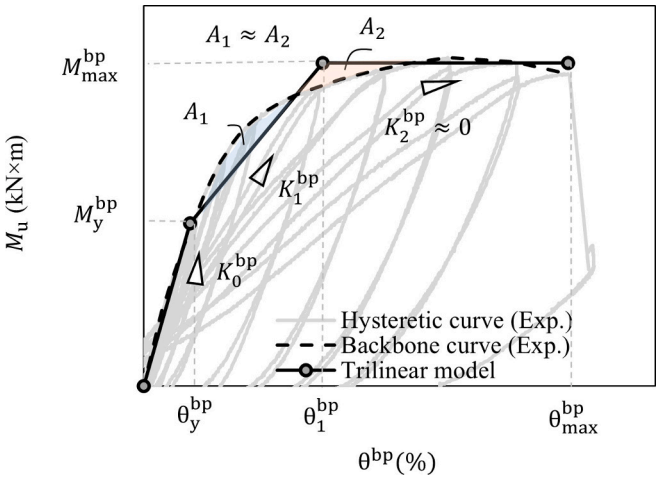

Fig. 2. Trilinear model for the idealization of the moment versus rotation response of ECBP (schematic).

joint. The mechanism to transfer the force and moment applied to the steel plate depends on the axial load-moment interaction. For instance, tensile loads are induced in the anchor rods along with bearing stresses in high loading eccentricity (i.e., high moment relative to axial compression) scenarios, while for lower eccentricities, the moment may be resisted entirely by bearing stresses.

Referring to Fig. 1, it is important to note that in the context of this paper, the elastic deformation of the column Δ^{col} is not considered in the model development. In most experiments, the lateral force and cantilever displacements $\Delta^{cantilever}$ are recorded, and then the test data is processed to remove this deformation, retaining only the connection rotation θ^{bp}. In these experiments, the moment-rotation (M-θ) curves were recovered from the load-deformation response as shown in Eqs. (1) and (2).

$$M_u = V_u L_{col} \tag{1}$$

$$\theta^{bp} = \left(\Delta^{cantilever} - \frac{V_u L_{col}^3}{3 E_{col} I_{col}}\right)\frac{1}{L_{col}} \tag{2}$$

where V_u and M_u are the measured horizontal load and moment at any loading step, respectively. L_{col} is the column length, θ^{bp} is the measured rotation of the ECBP, E_{col} is the modulus of elasticity of the column, and I_{col} is the moment of inertia of the column in the direction of bending. Once the moment-rotation response is recovered as above, a trilinear model is used to idealize the backbone of these M-θ curves and parametrically represent them. Such a model is sufficient to represent the ductility, stiffness, and strength degradation of the connections, considering the results of Rodas et al. [33]. Fig. 2 illustrates the key assumptions of the trilinear model and its basis. In this study, the rotation θ^{bp} is expressed in a percentage unit, like is commonly done for inter-story drifts of MRFs; this aims to highlight what element between the column and ECBP is expected to yield first in these systems (e.g., where the frames roughly yield with inter-story-drift values of 1 %), as highlighted in Section 7; this unit can be converted to any other (i.e., mrad) considering the background presented in this section. The overlaid hysteretic curve corresponds to a half-cycle of loading (of a representative test from Gómez et al. [16]). It is important to note here that the backbone curve represents the implied monotonic response of the connection, concerning which degradation may be computed and simulated, and not merely the envelope of the hysteresis curve, which may be an artifact of the loading history. The trilinear idealization shown in Fig. 2 is defined by the parameters summarized in Table 1.

Several models have been developed over the past three decades to characterize M-θ curves for ECBP, including analytical models proposed by Torres-Rodas et al. [33] and Latour and Rizzano [10], Stamatopoulos and Ermopoulos [34], and Abdollahzadeh and Ghobadi [35]. Some notable limitations of these analytical models in characterizing M-θ curves are addressed in this study; these include:

Table 1
Summary of the model parameters for moment-rotation curves of ECBP.

Modeling parameter	Description
θ_y^{bp}	Yield rotation. This deformation marks the end of the initial nearly linear response. This parameter normally coincides with the first yielding of any connection component (e.g., the plate on the compression/tension side or the anchor rods in tension).
θ_1^{bp}	Intermediate rotation is associated with the beginning of the plastic plateau. Experiments carried out by Gomez et al. [16] indicate that this parameter is associated with the yielding of a second component in the joint (e.g., if the plate yielded first in compression, then a subsequent yielding of the plate or anchor rods in tension). From a practical standpoint, this parameter is defined so that areas A_1 and A_2 (see Fig. 2) are equal.
θ_{max}^{bp}	Ultimate base rotation, which indicates a failure event (e.g., a sudden loss of strength), is noted. This failure is usually due to a fracture of the anchor rods or welds.
M_y^{bp}	Yield resisting moment. This is the moment associated with the yield rotation of the connection and, therefore, with the first yielding component. Regardless of which component yields first (e.g., plate or anchor rods), there is a sudden change in the load-displacement relationship of the joint after this flexural demand is reached.
M_{max}^{bp}	Ultimate resisting moment. This moment is linked to the second yield rotation θ_1^{bp} (or yielding component). This moment is maintained until the ultimate base rotation is attained when an abrupt loss of strength is noted.

- The rotational deformation limits associated with ECBP response (and summarized in Table 1) are somewhat challenging to describe mechanistically because the interaction of several components controls them; as a result, they are characterized based on empirical observations entirely. This results in a loss of accuracy, e.g., the model proposed by Kanvinde et al. [14] introduces subjectivities in the prediction of rotational parameters that result in an overestimation of the initial stiffness of this connection. Likewise, an overestimation of K_0^{bp} by Eurocode 3:1–8 is reported by Latour et al. [15].
- The number of tests used to validate some predictive models is limited for their generalization and use in guidelines and standards; note Latour and Rizzano [32] (15 data points), Kanvinde et al. [14] (15 data points), and Stamatopoulos and Ermopoulos [34] (8 data

points). Moreover, some of these experiments were devoted to investigating specific parameters (e.g., ultimate strength or initial stiffness of ECBP) or connection configuration, and do not report the full range of parameters required to define M-θ curves.
- The influence of axial loads on the rotational capacity of connections is not considered in some published models (e.g., Abdollahzadeh and Ghobadi [35]). This contrasts with the findings of Kanvinde et al. [14], Trautner et al. [19], and Mohabeddine et al. [36]; wherein it is noted that the ECBP system's rotational behavior depends on the columns' rotational capacity and the Axial Compression Ratio *ACR*.

3. A new database of experiments on ECBP subjected to flexure and axial loads

As part of this current study, a compendium of experimental data was assembled and made publicly available at https://cbp-db-modelling.utb.edu.co/search. The database contains information from tests to facilitate the estimation of individual parameters (e.g., θ_{max}^{bp}) in addition to the full range of M-θ curves of ECBP connections. The following test variables are typically defined in each experimental study (see Table 2):

- Column section and size: wide flange (e.g., American W profiles and European HEA and HEB profiles) or Hollow Structural Sections (HSS).
- Loading type: monotonic, cyclic, and constant or variable axial load.
- *ACR* from 0 % (no axial loads) to 63 %. The *ACR* is calculated as P_u / (A F_{yc}), where P_u is the axial force at the base of the column, A is the cross-sectional area of the column, and F_{yc} is the yield flexural strength of the column.
- Bolt pattern: 1 row-1 bolt, 2 rows-4 bolts, 2 rows-6 bolts, or 3 rows-8 bolts.
- Thickness of plate t_p and diameter of bolts D_b: 12 mm to 32 mm.
- Bolt-installation method: pretensioned, cast-in-place, epoxy drilled, or undercut bolts.
- Measured material properties (i.e., F_{yc}, yield stress of the plate F_{yp}, and ultimate strength of the bolts F_{ub})

The database contains results from a total of 84 specimens. The M-θ curves from the tests performed by the second author of this article ([16,29]) were provided in digital format, while the other experimental curves were graphically digitized. ECBP modeling parameters (e.g., those summarized in Table 1) values were determined by shaping trilinear curves to match the experimental curves (i.e., the backbone of cyclic or monotonic); this methodology is similar to that used by Lignos and Krawinkler [37] for other types of load-deformation curve matching.

4. Selection of predictor variables for non-mechanics-based models

As mentioned above, this work aims to provide predictive equations to characterize the nonlinear rotational behavior of ECBP connections. For this purpose, the trilinear model shown in Fig. 2 is used, defined by the five parameters shown in Table 1; of these, 2 are strength parameters (M_y^{bp} and M_{max}^{bp}), and 3 are deformation parameters (θ_y^{bp}, θ_1^{bp} and θ_{max}^{bp}). Previous work (i.e., Gómez et al. [16], Kanvinde et al. [29], Trautner et al. [19]) indicates that the mechanistic model developed by Drake and Elkin [28] (adopted by AISC Design Guide 1 [12]) provides fairly accurate estimates of both the strength parameters across a range of ECBP configurations. In addition to these parameters, previous work by Kanvinde et al. [14] shows that the yield rotation θ_y^{bp} can also be estimated using the mentioned mechanistic models. As a result, this approach (as discussed in a subsequent section) estimates them. On the other hand, the deformation parameters (θ_1^{bp}, θ_{max}^{bp} and, optionally θ_y^{bp} for

Table 2
Summary of specimens and loading types in the experimental database.

Study #	Authors	No. of spec.	Parameters investigated	Primary goals
1	You and Lee [38]	7	• Bolt pattern • Rod type • Stretch length	Examine the influence of anchor-rod layout on the performance of ECBP
2	Trautner et al. [19]	9	• Setting method • Anchor details • Base plate details • *ACR*	Study the performance of ECBP, including yielding anchors
3	Trautner et al. [39]	8	• Anchor type • Use of leveling nuts • Stretch length	Study the performance of ECBP, including yielding anchors
4	Kanvinde et al. [29]	8	• Bolt pattern • Column size • Plate dimensions	Investigate the adequacy of the design method proposed in the AISC Desing Guide 1 [12] for alternate configurations, then refine this method for these connections.
5	Latour et al. [15]	4	• Bolt pattern • Column size • Plate dimensions • *ACR*	Evaluate the accuracy of the models adopted by Eurocode 3 [40] for predicting the rotational stiffness and strength of ECBP
6	Demir et al. [41]	1	• M-θ curve of one ECBP	Examine the inelastic behavior of different types of column-base plates
7	Choi and Choi [42]	2	• Loading type • t_p	Study the inelastic behavior of ECBP
8	Gómez et al. [16]	7	• Loading type • *ACR* • Bolt pattern and t_p	Propose a refined design method for predicting the strength of ECBP, overcoming the limitations of existing methods
9	Fahmy et al. [43]	1	• M-θ curve of one ECBP	Investigate the seismic response of ECBP
10	Burda and Itani [44]	6	• Plate dimensions • t_p	Analyze the influence of the stiffness of ECBP on the behavior of steel moment frames
11	Jaspart and Vandegans [3]	6	• *ACR* • t_p	Compare experimental strength and stiffness with the predicted response of ECBP using a component-based approach
12	Wheeler et al. [45]	8	• Plate dimensions	Calibrate a rotational-strength model for bolted end-plate connections
13	Wald et al. [46]	4	• Loading type • *ACR*	Outline the use of the component method for predicting the strength and stiffness of ECBP
14	Thambiratnam and Paramasivam [47]	9	• *ACR* and moment • t_p	Study the failure mode of ECBP subjected to axial load and moment
15	Picard and Beaulieu [20]	4	• Column section	Determine the flexibility of ECBP
	Total Tests	**84**		

comparison with the mechanistic-based approach) are developed through regression. In this regard, the predictor variables (i.e., input parameters from the tests) used for these regressions require careful selection to achieve maximum accuracy and mitigate overfitting (Chatterjee and Hadi [48]; Aladsani et al. [49]). In this study, the selection of predictor variables is codependent on the regression process. This section summarizes the selection method, which corresponds to the filter method suggested by Sun et al. [50]. The final selection of variables for each predictive equation was made after the regression process, as detailed in Section 5.

4.1. Identification of relevant predictor variables

The first step identified potential variables from a behavioral standpoint. To provide context for this exercise, Table 3 summarizes test variables that various researchers have documented during their test programs (these test programs are summarized previously in Table 2). Referring to Table 3, a total of 41 variables (representing aspects of the specimen configuration, materials, and loading) have been proposed, mostly following the aims of the respective studies. It is unfeasible to use all these parameters in the development of our approaches. Thus, the main aim of this section is to reduce this large set of variables to a reduced set of variables that are most relevant to predicting the response of the ECBP connections. The following sections describe the process of selecting these variables.

4.2. Criteria for selection of predictor variables

The selection of predictor variables can be conducted either stochastically or mechanistically (e.g., by closely examining and analyzing experimental results), which requires a high quantity of high-quality data, as discussed by Obuchi and Kabashima [51]. Regarding regression models on ECBPs, a combined selection method including both ways has been considered due to some restrictions inherent to these connections: i) experimental results are still relatively limited, ii) many variables physically influence their behavior (consequently, purely statistical methods yet are not feasible), and iii) a comprehensive understanding of their mechanics (as introduced in Section 1) justifies carefully utilizing engineering judgment and behavioral insights in the variable selection process. Recently, Kabir et al. [52] have proposed an exploratory data-driven approach for identifying the failure mode of ECBPs using a combined selection method. Although this work is pioneering and a contribution from a research standpoint, some limitations are identified and overcome: i) the vertical load is not considered, which has been shown to have a significant influence on the connection's behavior (Gómez et al. [16] and Torres-Rodas [33]), ii) variables show substantial variability within the database; for instance, ECBP with pretensioned bolts like those tested by Trautner et al. [19,39] generate a self-centering effect, which is physically distinct from the response of other configurations; similarly, irregular bolt configurations in specimens produce different results to regular ones. Two steps were used in the selection process. These include primary filtering (see Subsection 4.2.1) aimed at reducing the number of predictors leveraging the experimental evidence and secondary filtering (see Subsection 4.2.2) to minimize collinearity between predictors.

Table 3
Summary of potential predictor variables.

Publication (s)	Model objective	Variables
Drake and Elkin [28], Kanvinde et al. [29]	Strength	• Plate dimensions: width B, length N, and t_p • Bolt dimensions and layout: cantilever distance of the plate m, edge distance g, and section area of a bolt group A_{rod} • Material properties: E_{col}, F_{yp}, F_{yc}, concrete compressive strength f'_c and F_{ub} • Internal forces: P_u and tensile force in anchor rods T • Column dimensions: height of the column section d, width of the column flange b_{fc}, thickness of the column flange t_{fc}, L_{col}, I_{col}, and Δ^{col} • Other variables: bearing length on the compression side Y and areas A_2 and A_1
Kanvinde et al. [14]	Stiffness	• Material properties: modules of elasticity of bolts, plate, and concrete (E_b, E_p, and $E_{concrete}$, respectively); shear modulus of the plate G_p • Dimensions and geometric properties: stretch length and diameter of bolts (L_b^{total} and D_b, respectively); moment of inertia and shear area of the plate (I_p and A_p, respectively); depth of the concrete footing d_{foot}
Latour et al. [32]	Ductility	The thicknesses of grout pad, washers, and nuts (t_g, t_w, and t_n, respectively); the effective width and length of a T-Stub (b_{eff} and l_{eff}, respectively)
Latour et al. [10]	Cyclic behavior	The yield stress of the bolts F_{yb}. The width of the column flange and web fillet welds (S_f and S_w, respectively). The distance between bolts along the weak and strong direction of the column (B_0 and L_0, respectively)
	Sum	41 variables

In addition to the potential variables selected from published models (see Table 3), two potential predictors (e.g., L_{col}/d and m/t_p) were included based on a closer examination of experimental results. Regarding the former, the ratio of the column length (measured between two inflection points, e.g., L_{col} in Fig. 1 is doubled for a cantilever setting) to the section height provides some rationale for considering the slenderness of the column, as observed from experiments by Kanvinde et al. [29]. On the other hand, the ratio m/t_p was conveniently selected as a potential predictor to consider the effect of thinner plates on the rotational deformation of these joints, where $m = (N - d) / 2$ (see Fig. 3). The effect of this parameter has been previously observed by Gómez et al. [16] and Burda and Itani [44], and is noted in the greater ductility with thinner plates than thicker ones. Apart from this, analytical (Latour and Rizzano [10]; Kanvinde et al. [14]) and experimental (Jaspart and Vandegans [3]) findings have revealed the significant influence of axial loads on the initial stiffness of ECBP. Low axial loads are expected to reduce the initial stiffness of ECBP, whereas high axial loads tend to increase the initial stiffness of these connections. Based on these findings, *ACR* was selected as a potential predictor.

Regarding Fig. 3, since the linear regression lines are not horizontal (as explained later in Subsection 4.2.2), this shows a linear dependence of the yield and ultimate rotation parameters on the ratio m/t_p, indicating greater ductility of the ECBP as this ratio is higher. The predictor variables after primary filtering (twelve) are F_{yb}, F_{yp}, N, B, t_p, D_b, A_{rod}, I_p, A_p, L_{col} / d, m/t_p, and *ACR*. These variables were reduced from the 41 shown in Tables 3 to 12, listed next; such variables were filtered again, as explained in Subsection 4.2.2.

4.2.1. Primary filtering of predictor variables

As explained above (see the introduction to Subsection 4.2), the primary filtering of variables was conducted based on a detailed analysis of all the studies summarized in Table 2 and Table 3, considering the effects of these variables on the test response, as documented by the respective author. For instance, the influence of d_{foot}, b_{fc}, t_{fc}, t_w, t_n, g, B_0, and L_0 on connection behavior has not yet been reported as significant. Therefore, they are neglected as predictor variables. On the other hand, the experimental results of Trautner et al. [19] and You and Lee [38] display that D_b and A_{rod} directly influence the yield moment and rotation of ECBP. Likewise, the well-known importance of F_{yb}, F_{yp}, N, B, and t_p in predicting the response of ECBP can be corroborated by the analysis of the results of Gómez et al. [16], Trautner et al. [39] and Latour et al. [15]); hence, they remain as predictors.

4.2.2. Secondary filtering of predictor variables

Once the primary filtering has been conducted, secondary filtering is

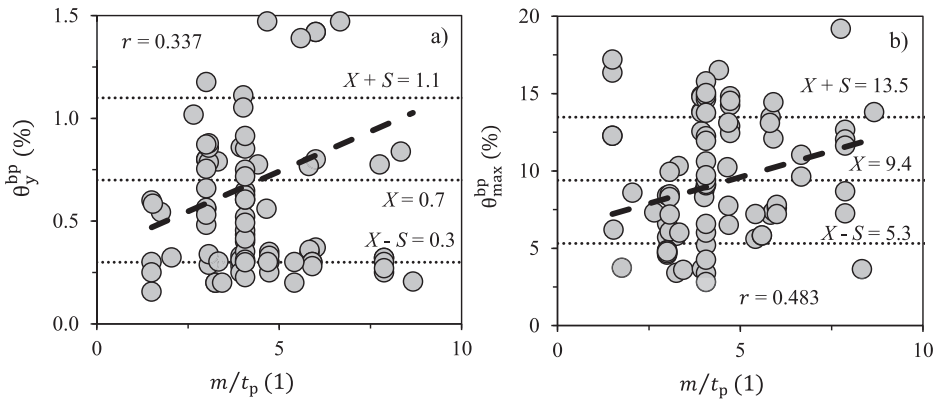

Fig. 3. Scatter plots and linear regression between the yield rotation parameter and the ratio m/t_p.

Table 4
Pearson's r between collinear predictors and the deformation parameters in simple linear regressions.

Parameter	D_b	A_{rod}	B	t_p	I_p	A_p
			|r|			
θ_y^{bp}	0.051	0.053⁺	0.047	0.204*	0.106	0.107
θ_1^{bp}	0.221	0.222⁺	0.009	0.199*	0.135	0.144
θ_{max}^{bp}	0.189	0.314⁺	0.028	0.194	0.202*	0.141

⁺ The largest value between A_{rod} and D_b
* The greatest value between I_p, A_p, B, and t_p

carried out based on simple linear and correlational analysis. The main objective of this evaluation is to avoid collinear predictors, retaining only the most relevant variables from a predictive standpoint. This step directly identified collinearities between predictors from their functional/mathematical description. For instance, in the equations for A_{rod} ($= \pi D_b^2 / 4$), I_p ($= B\ t_p^3 / 12$), and A_p ($= B\ t_p$), two groups of collinear variables are distinguished: i) Group A: A_{rod} and D_b, ii) Group B: I_p, A_p, B, and t_p. Therefore, some of these predictors shall be neglected. For this purpose, an exclusive selection between A_{rod} and D_b was considered to avoid collinearity in the former group. In the latter group, three exclusive options for selecting predictors were entailed: i) B and t_p, ii) I_p, and iii) A_p. The following two evaluation metrics were used in this step:

- Visual analysis of scatter plots and slopes of linear regression lines. A linear regression analysis was performed individually between each deformation parameter in the database (i.e., θ_y^{bp}, θ_1^{bp}, and θ_{max}^{bp}), and each of the filtered variables in Subsection 4.2.1, to illustrate their dependence or correlation. Regarding these regressions (for example, see Fig. 3), the horizontal regression lines indicate that the modeling parameters do not depend on the variable evaluated. On the other hand, the steeper (ascending or descending) the regression line is, the more predictive significance the variable might have. In either case, this analysis is only qualitative (e.g., because the units of the slope of the simple regression lines will depend on each variable under analysis). Therefore, the following coefficient is also considered to complement the visual analysis of scatter plots.
- Pearson's correlation coefficient r. This coefficient is a number between −1 and 1. The closer r is to −1 or 1, the stronger the linear relationship between the two variables evaluated.

The process for the second filtering can be summarized as follows:

1. The Pearson's r is calculated between the deformation parameters (i.e., θ_y^{bp}, θ_1^{bp}, and θ_{max}^{bp}) and each of the collinear predictor variables (e.g., A_{rod}, D_b, I_p, A_p, B, and t_p), as summarized in Table 4.

As observed in Table 4, A_{rod} has a higher correlation than D_b with the three deformation parameters. Therefore, following the introductory discussion to this subsection, D_b was excluded from group A. In group B, t_p shows a higher correlation than B, I_p, and A_p for yield rotations (e.g., θ_y^{bp} and θ_1^{bp}), while a slightly lower correlation than I_p for the ultimate rotation θ_{max}^{bp}. Overall, t_p shows the best potential predictive capacity for the deformation parameters in group B; hence, this is selected as a predictor. The predictor variables selected after this sub-step (nine) are F_{yb}, F_{yp}, N, L_{col}/d, m/t_p, ACR, B, t_p, and A_{rod}.

2. In the previous sub-step, a correlational analysis was conducted among the nine filtered predictors. Then, the Pearson coefficients were calculated and analyzed to confirm or exclude the nine filtered variables, following the recommendations of some authors (Aladsani et al. [49]; Sun et al. [50]).

As described by Nettleton [53], a coefficient between 0.7 and 0.9 indicates a strongly linear relationship between two variables. Meanwhile, for values lower than 0.7, a moderate or weak relationship is expected. Table 5 shows the r coefficients between the selected predictor variables. The table shows that most values correspond to low or

Table 5
Pearson's coefficient between predictor variables.

Variable	L_{col}/d	F_{yb}	N	m/t_p	B	F_{yp}	t_p	A_{rod}	ACR	1.000
L_{col}/d	–									0.750
F_{yb}	0.265	–								0.500
N	0.225	0.249	–							0.250
m/t_p	0.274	0.257	0.342	–						0.000
B	0.201	0.204	0.900	0.158	–					
F_{yp}	0.731	0.385	−0.030	0.242	0.005	–				−0.250
t_p	0.132	0.022	0.535	−0.413	0.535	−0.244	–			−0.500
A_{rod}	−0.031	0.272	0.491	−0.176	0.556	−0.006	0.539	–		−0.750
ACR	−0.533	−0.251	−0.295	−0.089	−0.289	−0.385	−0.226	−0.212	–	−1.000

Table 6
Examined range and physical importance of selected predictor variables.

Predictor variable	Min	Max	Physical importance
F_{yb} (MPa)	240	830	The results of Trautner et al. [19,39] indicate that the greater F_{yb} is, there is a tendency for θ_{max}^{bp} to decrease and M_{max}^{bp} to increase.
F_{yp} (MPa)	235	354	There is no experimental evidence of the influence of F_{yp} on the rotational strength of ECBPs. However, a behavioral analysis suggests that it could have a prominent influence on the strength when the failure mechanism involves plate yielding on the tension side.
N (mm × 10^2)	2.00	6.09	The results of Burda and Itani [44] suggest that B and N have a linear relationship with the connection ductility, e.g., the greater N while other dimensions are constant, the larger the rotation θ_{max}^{bp}.
B (mm × 10^2)	1.78	6.09	
t_p (mm)	9.00	69.8	Direct experimental remarks cannot be made about the influence of t_p on the modeling parameters without contextualizing its interaction with other variables. However, the analysis of the results of Gomez et al. [16] points out that when the first yielding occurs in the plate-in-compression, the elastic parameters (θ_y^{bp} and M_y^{bp}) have linear codependency with t_p. Analogously, when the first yielding occurs in the plate-in-tension, M_y^{bp} and M_{max}^{bp} are dependent on t_p (see Burda and Itani [44]).
A_{rod} (mm^2 × 10^2)	2.26	23.7	Similar to t_p, explicit observations from experiments cannot be made for A_{rod} without the context of other variables. Nonetheless, from a behavioral standpoint, there seems to be a linear relationship between A_{rod} and the yield line pattern (and so the capacity of the connection in general).
ACR (%)	0.00	72.1	Low axial loads tend to reduce the initial stiffness of the connection, while high axial loads are expected to increase the mentioned stiffness.
L_{col}/d (1)	6.00	50.4	Based on the experiments of Latour et al. [15] and Gómez et al. [16], the larger the L_{col}/d, the larger the deformation (θ_y^{bp} and θ_{max}^{bp}) and strength (M_y^{bp} and M_{max}^{bp}) parameters. Apparently, these cases represent weak column-strong base behavior.
m/t_p (1)	1.50	8.67	The lower m/t_p, the higher the strength parameters, the lower θ_{max}^{bp} (e.g., ductility).

moderate linear correlation between predictors, except between B and N ($r = 0.900$). Nonetheless, a closer examination of the behavioral insights of ECBP indicates that these two variables do not have linear relationships. The reason for this high value must merely be a coincidence; commonly, the base plate is defined as square, and then B is as N. In either case, the variables in the equation are centered and normalized to reduce multicollinearity, as described later in Section 5. To conclude, the nine selected variables listed below were included in the multivariate regression process outlined in Section 5. The predictor variables after secondary filtering (nine in total) are F_{yb}, F_{yp}, N, B, t_p, A_{rod}, L_{col} / d, m/t_p, and ACR.

4.3. Physical relevance of selected predictor variables

This subsection briefly discusses the physical meaning of the nine predictor variables selected after secondary filtering from observations in the experiments compiled in the database (see Section 3). Table 6 summarizes the discussion and shows the range of these variables examined in the various experimental studies. It is worth noting that an introductory discussion of the variables ACR, L_{col}/d, and m/t_p (innovatively proposed in this study) is presented in Subsection 4.2.1.

5. Predictive equations for the modeling parameters

In this section, predictive equations for the parameters of the M-θ curves of ECBP are presented. These define the response of the trilinear backbone model (see Section 2 and Fig. 2). As mentioned above (Section 4), non-mechanistic (i.e., regression-based) equations were determined for the rotational parameters (mandatory use for θ_1^{bp}, θ_{max}^{bp} while optional use for θ_y^{bp}), whereas a mechanistic-based model (e.g., that proposed in AISC Design Guide 1 [12]) is adopted for calculating the strength parameters (M_y^{bp} and M_{max}^{bp}) and the yield rotation parameter θ_y^{bp}. A combination of regression- and mechanistic-based equations is aimed at overcoming some limitations of previous predicting models (see Section 2), meanwhile achieving generalizability for inclusion in guidelines and use by practitioners.

5.1. Regression-based predictive equations

The entire procedure followed to determine these equations is summarized below:

- The measured values of properties of specimens and their backbone M-θ curves were compiled into the database, as explained in Section 3.
- A trilinear M-θ curve was defined for each backbone curve, as explained in Section 2.
- The most significant predictor variables were selected, as explained in Section 4.
- Initially, conventional least-square multiple-linear regression was employed to predict all the modeling parameters. However, heteroscedasticity was detected on their residual plots, indicating model deficiency. Consequently, variable transformations (e.g, weighted least-square and centering) were used to address this issue, as recommended by Chatterjee and Hadi [54]. On one hand, the former transformation aims to eliminate heteroscedasticity; after a careful examination, it was noticed that ACR has a meaningful zero value (Table 6) from mechanistic and stochastic standpoints and then generates an arithmetic issue, i.e., a zero divisor. On the other hand, centering refers to subtracting the mean (or another constant value within the observed range) from every observation; researchers commonly use this transformation to reduce multicollinearity accurately, and in the context of this study, this also eliminates the issues above. It is worth noting that centering against the mean is only recommended when variables do not have meaningful zero values

Table 7
Regression coefficients for non-mechanics based equations.

Parameter	Regression coefficients (1)										
	C	β_0	β_1	β_2	β_3	β_4	β_5	β_6	β_7	β_8	β_9
θ_y^{bp}	1.0	7.568×10^{-3}	−0.143	0.000	−0.236	0.339	0.000	0.955	0.116	-6.000×10^{-3}	−0.025
θ_{max}^{bp}	1.0	1.607	0.000	−0.363	−2.631	1.988	0.745	0.000	1.198	−0.040	0.103
θ_1^{bp}*	1.0	2.754×10^{-2}	0.007	0.000	0.785	0.358	−0.920	0.855	0.000	−0.037	−0.048

* For pretensioned bolts, $\theta_1^{bp} = 0.51\ \theta_{max}^{bp}$

Table 8
Yield moment of the main components of ECBP.

Component	Connection side	Formulation	Eq.
Plate	Tension	$M_{yp}^{tension} = 4\,T_{yp}(m-g)$ (large eccentricity)	(5)
	Compression	$M_{yp}^{comp\text{-}small} = P_u\,\frac{(N-Y1)}{2}$ (small eccentricity), where $Y1 = \left\{\begin{array}{l} \frac{2.25P_u m^2}{F_{yp}Bt_p^2} \text{for } Y1 \geq m \\ \frac{2B}{P_u}\left[\frac{P_u m}{B} - F_{yp}\left(\frac{t_p}{2.11}\right)^2\right] \text{for } Y1 < m \end{array}\right\}$	(6)
		$M_{yp}^{comp\text{-}large} = f_{max}\,B\,Y2_p\left[(N-g) - \frac{Y2_p}{2}\right] - P_u\left(\frac{N}{2}-g\right)$ (large eccentricity), where $Y2_p = \left\{\begin{array}{l} m \pm \frac{\sqrt{(f_{max}m)^2 - 2f_{max}\left(\frac{t_p}{2.11}\right)^2 F_{yp}}}{f_{max}} \text{for } Y2_p < m \\ m \text{for } Y2_p \geq m \end{array}\right\}$	(7)
	General rule	$M_{yp} = M_{yp}^{comp\text{-}small}$ (small eccentricity)	
		$M_{yp} = \left\{\begin{array}{l} M_{yp}^{comp-large} \text{for } T_{yb} \leq T_{yp} \\ min\left(M_{yp}^{comp-large} M_{yp}^{tension}\right) \text{for } T_{yb} > T_{yp} \end{array}\right\}$ (large eccentricity)	(8)
Anchor rods	Tension	$M_{yb} = P_u\frac{\left[\left(f+\frac{N}{2}\right)^2 - \left(\left(f+\frac{N}{2}\right) - Y2_b\right)^2\right]q_{max}}{2P_u} - f$ (large eccentricity), where $Y2_b = \frac{T_{yb}+P_u}{q_{max}}$	(9)

Table 9
Mechanics-based equations for the modeling parameters of ECBP.

Parameter	Formulation	Eq.
M_y^{bp}	$M_y^{bp} = \left\{\begin{array}{l} min(M_{yp}, M_{yb}) \text{if} T_{yb} \leq T_{yp} \\ M_{yp} \text{if} T_{yb} > T_{yp} \end{array}\right\}$	(10)
M_{max}^{bp}	$M_{max}^{bp} = max(M_{yp}, M_{yb})$	(11)
θ_y^{bp}	$\theta_y^{bp} = M_y^{bp}/K_0^{bp}$	(12)

Table 10
Performance metrics of non-mechanistic equations.

Parameter	Predictive equation	Predictive performance			
		n (1)	R^2 (1)	(Test/pred)$_{MEAN}$ (1)	(Test/pred)$_{CoV}$ (1)
θ_y^{bp}	(3)	63	0.41	1.04	0.43
θ_{max}^{bp}	(3)	56	0.46	1.05	0.33
θ_1^{bp}	(3)	46	0.59	1.03	0.32

Table 11
Performance metrics of mechanics-based equations.

Parameter	Predictive equation	Predictive performance			
		n (1)	R^2 (1)	(Test/pred)$_{MEAN}$ (1)	(Test/pred)$_{CoV}$ (1)
M_y^{bp} [+]	(10)	17[+]	0.56	0.91	0.26
M_{max}^{bp} [*]	(11)	12[*]	0.97	1.11	0.24
θ_y^{bp} [°]	(12)	14[°]	0.37	1.08	0.42

[+] The specimen W10 × 77 ([43]) generates an Out-of-Trend Data (OTD) for this parameter
[*] The column welds of specimens T1 to T6 ([44]) fractured before registration of M_{max}^{bp}
[°] The specimens T1, and T4 to T6 ([44]) generate OTD for Eq. (12)

Table 12
Summary of k-fold cross-validation of regression-based predictive equations.

Description	θ_y^{bp} (%)	θ_{max}^{bp} (%)	θ_1^{bp} (%)
$RMSE_{fold\ 1}$	0.28	4.09	0.75
$RMSE_{fold\ 2}$	0.66	5.45	0.80
$RMSE_{fold\ 3}$	0.52	3.64	1.00
$RMSE_{fold\ 4}$	0.30	1.93	1.11
$RMSE_{fold\ 5}$	0.23	2.68	1.20
$RMSE_{fold\ 6}$	0.21	3.11	1.01
$RMSE_{fold\ 7}$	0.33	2.58	1.67
$RMSE_{fold\ 8}$	0.18	3.02	1.56
$RMSE_{fold\ 9}$	0.37	2.55	–
$RMSE_{fold\ 10}$	–	–	–
$RMSE_{new\ data}$	0.34	3.23	1.14
In-sample $RMSE$	0.31	2.99	1.01
k	9	9	8
Training-testing split	56–7 (9 folds)	49–7 (2 folds) 50–6 (7 folds)	40–6 (6 folds) 41–5 (2 folds)
n	63	56	46

and, then another constant value within the variables observation range may be selected, considering a particular research objective (see Dalal and Zickar [55] and Enders and Tofighi [56]). Considering all the above and after several centering alternatives, adding the unity and weighting to ACR values in this study shows the best-fit and stable regressions.

- Subsequently, various multiple-nonlinear regressions (e.g., quadratic, logarithmic, Poisson, and exponential equations with original and transformed variables) were evaluated. Exponential equations with transformed variables correlated better with the experimental data than others. This better correlation of nonlinear functions aligns with experiments because plate yielding in the joint occurs at initial loading stages, as observed in most test campaigns reported in the dataset.

- Finally, regression equations were defined through a backward elimination process (for the rotational parameters), initially considering all the selected predictor variables. The minimum statistical significance of predictions is defined as 95 %.

The JASP© software [57] facilitated the statistical simulation process. Chatterjee and Hadi [54] indicate that the variables that will ultimately be selected for regression models should be linked to the functional forms of the equations. As explained above, the non-mechanistic equations for predicting the rotational parameters of ECBP are characterized by a nonlinear form, as shown in Eq. (3). As described above, the variables in the equation are centered (to the constant *C*) and normalized (to the *ACR*-values) to avoid computational inaccuracies and eliminate heteroscedasticity, respectively.

$$Y = \beta_0\left(\frac{L_{col}}{d}+C\right)^{\beta_1}\cdot(F_{yb}+C)^{\beta_2}\cdot(N+C)^{\beta_3}\cdot\left(\frac{m}{t_p}+C\right)^{\beta_4}\cdot(B+C)^{\beta_5} \cdot(F_{yp}+C)^{\beta_6}\cdot(t_p+C)^{\beta_7}\cdot(A_{rod}+C)^{\beta_8}\cdot(ACR+C)^{\beta_9}-C \quad (3)$$

where *Y* is the so-called response or dependent variable (e.g., the predictive modeling parameter in this work), and β_0 to β_n are the regression coefficients. The standardized type of coefficients is expressed in units of standard deviation, and these usually need conversion factors when predictors have different units. On the other hand, unstandardized coefficients reflect the original units of the predictors, which are considered suitable for practitioners to use. Therefore, this study presents the regression coefficients as unstandardized (see Table 7), reflecting the units reported in the database (see Table 6). Physical insights of these coefficients and the predictive performance metrics of the non-mechanistic equations are discussed in Subsection 6.1.1.

Regarding θ_1^{bp}, for the subset with pretensioned bolts (17 specimens), the sample size is not adequate to develop the same statistical analysis that was performed for the full dataset; for this case, θ_1^{bp} may be empirically predicted as 0.51 θ_{max}^{bp}, where θ_{max}^{bp} may be predicted with the corresponding predictive equation, as shown in Table 7.

5.2. Mechanics-based predictive equations

The well-known Rectangular-Stress-Block approach in the AISC Design Guide 1 [12] is adapted to characterize the moment-strength modeling parameters using the *P-M* interaction approach. Salient aspects of the adaptation are as follows:

- The AISC Design Guide 1 calculates the force in anchors and bending moment in the plate for a given axial load-moment (*P-M*) pair. Then, the minimum t_p to avoid yielding in the plate or reaching the ultimate stress of the anchors is computed, and, finally, the overall strength of the connection is back-calculated from this procedure. On the other hand, the *P-M* interaction approach calculates the moments in the connection that are associated with the yielding of each component; this procedure considers the Rectangular-Stress-Block assumption of the Design Guide; the axial load, dimensions (e.g., tp) and material properties of components are entailed as input variables.
- According to a comprehensive assessment (Gómez et al. [16]) of the above-cited Design Guide, such guidelines only give the method for estimating M_y^{bp}, and not for M_{max}^{bp}. The assessment report indicates that additional considerations must be included for predicting M_{max}^{bp}, i.e., mechanism-based consideration and yield selection versus ultimate stress of materials. For this purpose, the *P-M* interaction approach presented in this study selects the yield strength of ECBP components and includes a modification factor. In addition to the above, the tensile forces T_{yb} and T_{yp} are relevant to predict the rotational strength of ECBP according to the adopted approach; the former corresponds to the yielding of anchors and is calculated as $A_{rod}\ F_{yb,}$ while the latter, the tension in anchors that is associated with the yielding in the tensioned side of the plate and is characterized with Eq. (4).

$$T_{yp} = \left(\frac{t_p}{2.11}\right)^2 \frac{B\ F_{yp}}{f-\frac{d}{2}} \quad (4)$$

where *f* is the distance from the anchor rod group's centroid to the column's centroid (= (*N* - *d*) / 2 - *g*). The formulations to calculate the yield moment of each component are summarized in Table 8. It is worth noting that the variables in the definition of *Y*1 and *Y*2 (e.g, (5) and (6)) may seem circular; however, this is not true mainly because these have physical meaning (not a purely mathematical one) and thus, there is no inherent circularity.

- As mentioned in Table 1, the ultimate resisting moment M_{max}^{bp} is associated with the component that yields second. For instance, if the plate yields first, the abovementioned moment corresponds to the anchor yield moment (or vice versa).

The symbols in Table 8 are defined in the notation list. The modification factor in Eq. (5) (equal to 4) is regression-based, considering test results of 18 specimens in the database for which yielding in the plate due to tensile force in the bolts contributed to generating a failure mechanism (e.g., if $T_{yb} > T_{yp}$). For these cases, a membrane action is developed. The axial force-moment pair that produces the first yielding in the tensile side of the plate does not correspond to a capacity condition – only an increasing response due to membrane action as the plate rotates to large deformations (see Kanvinde et al. [29]), but a value of 4 provides good agreement with experimental results if this is indeed the failure mode. Finally, the formulations of the *P-M* interaction approach (see Table 8) can be used to predict the strength modeling parameters of ECBP and θ_y^{bp}, as summarized in Table 9.

The evaluation of the predictive performance of the equations in Table 9 is presented in Subsection 6.1.2. The calculation of θ_y^{bp} in the table (Eq. (12)) is calculated following the procedure proposed by Kanvinde et al. [14]. This procedure identifies (by iteration) the first degradation of the initial stiffness of the connection according to the current AISC Design Guide 1.

6. Evaluation and discussion of model performance

This section discusses the predictive performance of the equations presented in Section 5 (mechanistic and non-mechanistic). Subsection 6.1 is dedicated to predicting individual modeling parameters. Subsection 6.2 qualitatively compares the experimental backbone with predicted (trilinear) M-θ curves, whereas 6.3 presents a cross-validation test of the regression-based equations for out-of-sample prediction to examine the robustness of the predictions.

6.1. Prediction of individual modeling parameters

To evaluate the ability of the approach to predict individual modeling parameters of ECBP, the mean and Coefficient of Variance (CoV) of the test-to-predicted (test/pred) ratios, and the correlation coefficient R^2 are examined in this subsection. The greater the value of R^2, the greater predictive importance any equation could have; this is a number between 0 and 1. Concerning $(test/pred)_{MEAN}$, the closer this ratio is to unity, the better the predictive performance of any equation. Also, the lower the $(test/pred)_{CoV}$, the higher the performance. For regression-based equations, the test dataset on which the "predictive performance" is evaluated is identical to that used to fit the regression coefficients (exponents in Eq. (3)); consequently, a quality-of-the-fit is a more appropriate term.

6.1.1. Non-mechanics-based parameters

Table 10 shows the values of selected metrics to evaluate the quality-of-the-fit (e.g., the number of specimens n, $(\text{test/pred})_{\text{MEAN}}$, $(\text{test/pred})_{\text{CoV}}$, and R^2) of the non-mechanistic equations summarized in Table 7.

Referring to Table 10, the deformation parameters of ECBP predicted with non-mechanistic equations show a satisfactory fit to experimental ones, i.e., the values of $(\text{test/pred})_{\text{MEAN}}$ for all three deformation parameters are equal or smaller than 1.05. Apart from this analysis, the non-mechanistic equation for θ_y^{bp} (Table 7) shows relatively high values of regression coefficients for F_{yp}, m/t_p, N, L_{col}/d, and t_p, indicating a strong dependence on these predictor variables; this observation agrees with the physical remarks summarized in Table 6, e.g., the yield rotation depends on F_{yp} and L_{col}/d. On the analysis of the non-mechanistic equation for the ultimate rotation θ_{max}^{bp}, N and m/t_p are notably influential, such as remarked in by physical meaning (Table 6). Fig. 4 shows the scatter plots between predicted and tested values of the rotational parameters.

As shown in Fig. 4, the predicted rotational parameters of ECBP have a reasonable correlation with the measured parameters. The values of R^2 for the expected values of θ_y^{bp}, θ_{max}^{bp}, and θ_1^{bp} are 0.41, 0.46, and 0.59, respectively. In the same order, the average values of the test-to-predicted ratios are 1.04, 1.04, and 1.03; meanwhile, the CoVs of these ratios are 0.43, 0.33, and 0.32, respectively. These metrics indicate a good quality-of-the-fit of the non-mechanistic equations, especially for θ_1^{bp} and θ_{max}^{bp}.

6.1.2. Mechanics-based parameters

It is worth noting that some ECBP configurations in the database are not covered in the design philosophy of the AISC Design Guide 1 [12]. Some of these configurations are ECBPs with pretensioned bolts and those with bolts located behind the column flanges in the extended zone of the plate (e.g., according to European practice). Consequently, in this study, the strength parameters of 18 specimens consistent with those included in the Design Guide 1 were predicted, i.e., for configurations where only two bolt rows are presented in the direction of bending. These specimens (and the corresponding studies) are listed below, and the evaluation of their parameter predictions is summarized in Table 11. About pretensioned bolts (i.e., those with tensile pre-loads of around 30 % of $A_{rod} \times F_{yb}$), the studies by Trautner et al. [19,39] show that these specimens have notably lower M_{max}^{bp} than others in the entire dataset; strength equations for configurations with additional bolt rows are presented in Kanvinde et al. [29].

- Gómez et al. [16]: # 2, # 4, # 5, # 6, # 7.
- Kanvinde et al. [29]: # 1, # 2, # 3, # 4.
- Fahmy et al. [43]: W10 × 77
- You and Lee [38]: SR2, SR4.
- Burda and Itani [44]: T1, T2, T3, T4, T5, T6.

The prediction metrics in Table 11 indicate adequate performance of the mechanistic equations. For instance, the correlation coefficients for the modeling parameters M_y^{bp}, M_{max}^{bp}, and θ_y^{bp} are calculated as 0.56, 0.97, and 0.37, respectively; the mean values of test-to-predicted ratios are 0.91, 1.11, and 1.08 in the same order, while the corresponding CoV values of these ratios are 0.26, 0.24 and 0.42. Fig. 5 works complementary with Table 11; the figure compares predicted (using mechanistic equations) and measured values of strength parameters and θ_y^{bp}. The figure shows that the scatter plots of predicted versus tested strength parameters indicate a high-quality fit.

As shown in Fig. 5, although there are some Out-of-Trend Data (OTD) points for each modeling parameter (as indicated in Table 11), there is an explicit agreement between most predicted and tested data. Furthermore, the few disagreements can be reasonably explained by physical meanings, as follows: i) In Fig. 5a, the ECBP components of specimen W10 × 77 ([43]) are notably over-dimensioned for the size of the column when compared to regularly designed specimens according to the current version of the AISC Design Guide [12] ii) In Fig. 5b, the welds of some specimens fractured before the ultimate resisting moment iii) In Fig. 5c, the OTD seems to follow a line intersecting the main trend line; such data correspond to specimens for which the first yielding component is the steel plate on the tension side.

From the analysis of Table 10 and Table 11, the non-mechanistic and mechanistic predictive equations for θ_y^{bp} lead to similar and reliable results. The former is easy to use and shows good precision, so it can be used in any case, whether in the examined range shown in Table 6 or outside (as discussed later in Subsection 6.3). However, its generalizability (e.g., for use in design guidelines) could be questioned due to its regression-based nature. So, in such cases, the latter is more appropriate, even if Eq. (12) implies iteration of the current design approach in AISC Design Guide 1 (12]), as introduced in 5.2. In summary, for a design approach, the following procedure is suggested to calculate θ_y^{bp}: i) calculate T_{yb} and T_{yp}, ii) if $T_{yb} > T_{yp}$, then use the non-mechanics-based equation (Eq. (3)), and iii) if $T_{yb} > T_{yp}$, then utilize the mechanics-based equation (Eq. (12)); alternatively, Eq. (3) can also be used for comparison and verification in either case. Apart from θ_y^{bp}, it is worth stating that the prediction of the deformation parameters θ_1^{bp} and θ_{max}^{bp} is unfeasible by the mechanistic approach. Therefore, these parameters must be predicted with non-mechanics-based equations outlined in Subsection 5.1.

6.2. Prediction of the complete M-θ curves

In addition to examining the scatter plots for predicting individual parameters (see Subsection 6.1), a qualitative comparison between the full M-θ curves from the tests and based on the determined parameters is shown in Fig. 6 to assess the quality of the fit of predictive equations. The identical specimens and criteria for evaluating the predictive performance of mechanistic equations for individual parameters (see Subsection 6.1.2) were considered. Specific studies, including the component-based model proposed by Eurocode 3 [40], shall be carried out for specimens conforming to European practice. Overall, Fig. 6a to l show that the fit of the proposed models to the experimental curves is very

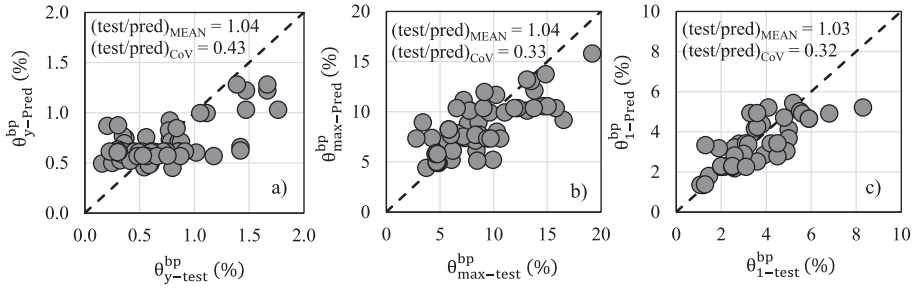

Fig. 4. Predicted vs. Tested values of the deformation parameters of ECBP using non-mechanistic equations.

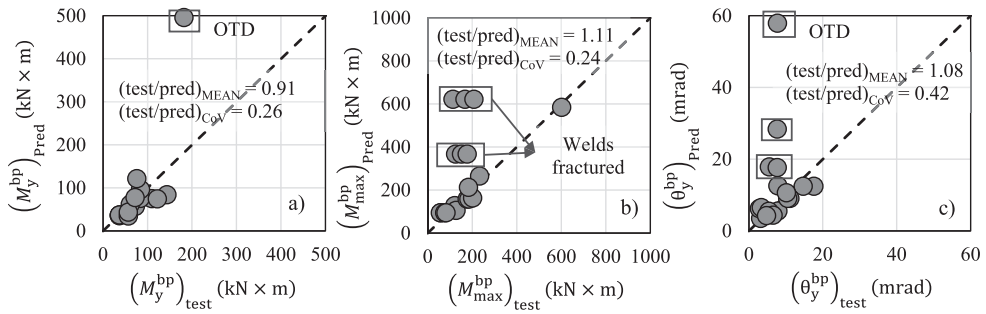

Fig. 5. Predicted vs. Tested values of the strength parameters of ECBP following the proposed approach.

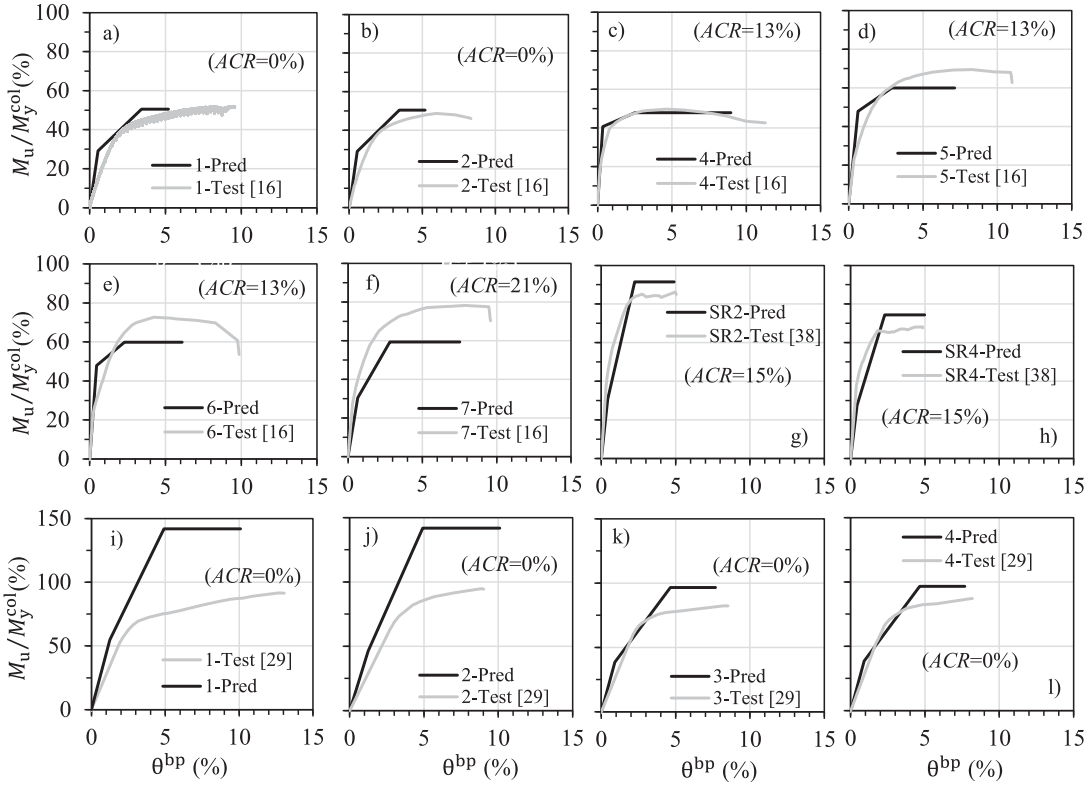

Fig. 6. Full-range of predicted M-θ curves for various specimens in the compiled database.

good. As an exception, an overestimation of the yield and ultimate strengths is observed for specimens 1 and 2 of Kanvinde et al. [29] (Fig. 6i and j); this overestimation can be explained by the fact that L_{col}/d for these specimens is notably larger than for others so that they can sustain more significant deformations (and loads) in a linear-elastic fashion.

A complimentary web-based tool was developed to calculate the modeling parameters of ECBP using the proposed regression-based equations for deformation parameters while mechanics-based expressions for strength parameters. The tool has an intuitive interface, which follows the same notation as in this paper. For illustration, Fig. 7 shows a screenshot of the tool, corresponding to the prediction of the modeling parameters for specimen 2 made by Gómez et al. [16]. In the figure, the input data are the nine predictor variables on the screen's left side. The output data are the predicted modeling parameters and the plot of the full range of M-θ curves of ECBP.

Although the regression-based equations proposed in this study (see Eq. (3) and Table 7) show satisfactory agreement with experimental results, they should be extrapolated with caution beyond the parameters range they were calibrated with (see Table 6). A performance evaluation for out-of-range is presented next.

6.3. Cross-validation test for non-mechanics-based eqs

A *k*-fold CV process is illustrated in Fig. 8, which has been used to evaluate the performance of the proposed equations against out-of-sample predictions. This procedure is a well-established technique for testing the predictive performance of regression models for new data (Sun et al. [50], Wakjira et al. [58]). This is particularly important in multivariable high-order regression models that are highly prone to overfitting (i.e., good predictions within the sample used to fit the data but poor predictions outside it). The *k*-fold CV consisted of randomly splitting the entire dataset (or the original training dataset) into testing and training subsets in a proportion close to 20 % / 80 %, respectively. The training subset was then used to train new regression models, while the testing one was used to test them. This process was repeated *k* times so that the testing subsets were mutually exclusive and approximately the same size as the previous folds. Finally, since the metric *RMSE* was used to evaluate the performance of the proposed regression models for new data (or out-of-sample data), the generalized performance of the

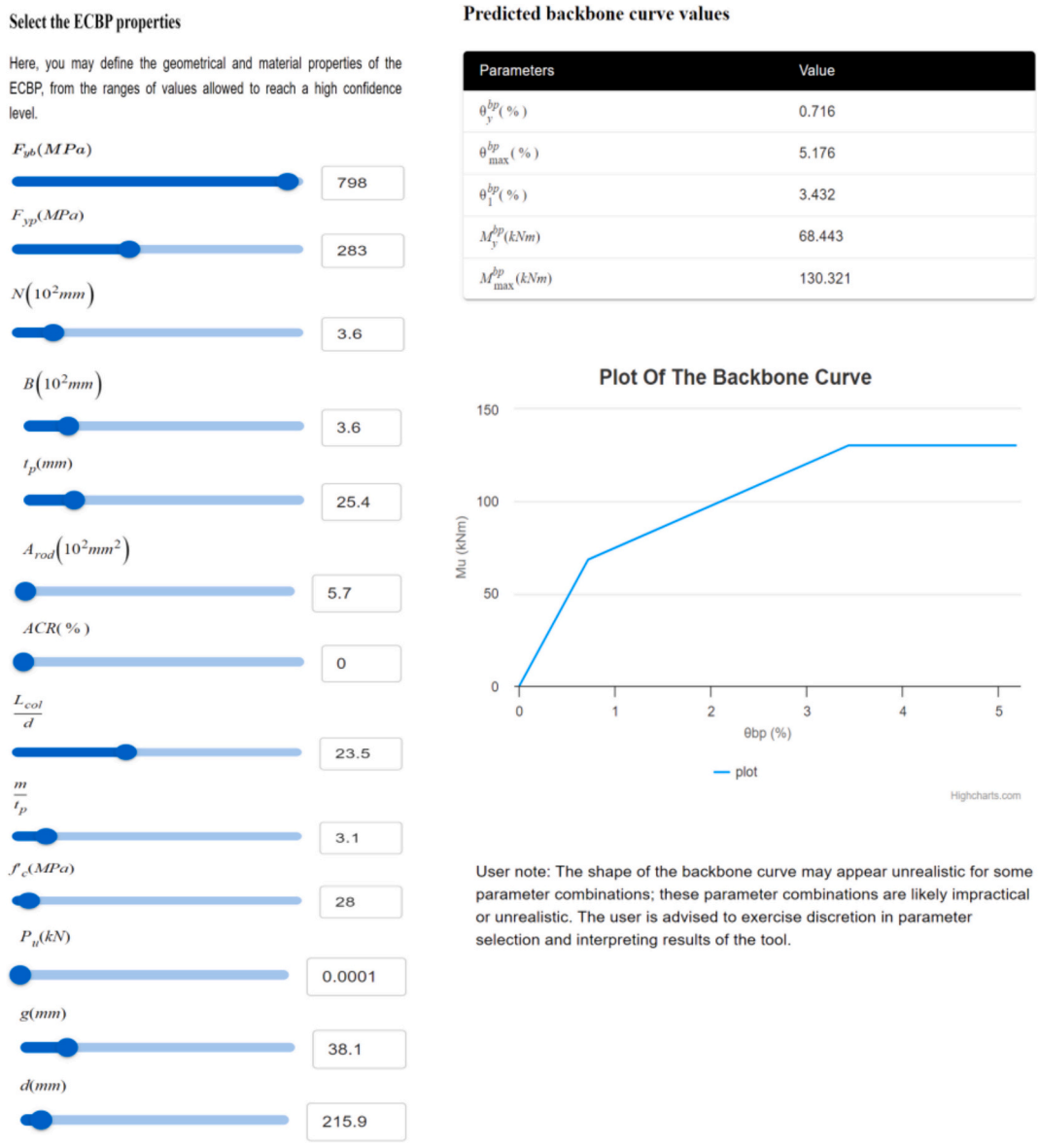

Fig. 7. Estimation of the modeling parameters for specimen 2 (Gómez et al. [16]) with the web-based tool.

models for new data is considered the average of the *RMSE* over the *k* folds. Overall, the out-of-sample performance of a model is better when the average *RMSE* is lower.

Table 12 summarizes the results of the CV test performed in this study. The in-sample *RMSE* for θ_y^{bp} is 0.31, while the out-of-sample $RMSE_{new\ data}$ is 0.34; both *RMSE* values are relatively low.

A closer examination of Table 12 indicates that all the models for the rotational modeling parameters also perform satisfactorily for new data. For instance, the predicted and tested modeling parameters have been compared and found to be reasonably similar. Therefore, the proposed models may provide the best estimates (e.g., even for out-of-sample predictions) until more specific tests are available.

7. Summary, conclusions, and limitations

This paper is focused on estimating modeling parameters of exposed column-base plates subjected to combined uniaxial flexure and compression loads, and their dependence on the main configurational variables for these connections. A dataset of 84 experimental test results was assembled and is available at https://cbp-db-modelling.utb.edu.co/search. A trilinear curve was adopted to represent the M-θ curves of the connections, given its feasibility of functionally representing the linear and inelastic behavior of the structural components. The modeling parameters can be grouped into rotational and moment-strength parameters; for the rotational ones, regression-based equations are proposed; for the strength parameters, the well-known mechanistic model adopted in the Design Guide 1 of the American Institute of Steel Construction is utilized. The selection of predictor variables for the regression-based models was carried out in three steps. First, potential predictor variables were preliminary selected from published mechanics-based models and test parameters. Secondly, the number of predictor variables was filtered considering experimental observations and their statistical significance. Third, predictor variables for each modeling parameter were determined using backward regression analysis. Best-fit predictive equations for modeling the connections are proposed, and their predictive performance is evaluated for in-sample (comparing against test data) and out-of-sample data (with a Cross-Validation process); the correlation matrix of predictors is employed to avoid collinearity. The main conclusions of this work are:

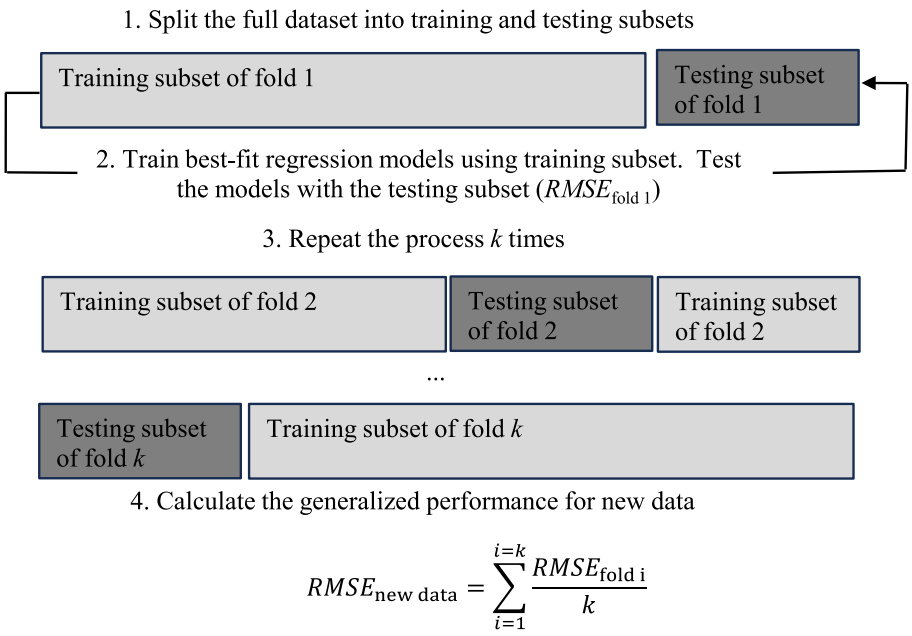

Fig. 8. Illustration of CV using k folds.

- When the proposed regression-based equations for the deformation parameters are used, the predicted first yield, intermediate, and ultimate rotations reliably fit the observed data. The plate length and thickness notably influence all the rotational parameters. At the same time, the design variables of the bolts (i.e., the cross-sectional area of a bolt group and their yield stress) mainly affect the ultimate rotation. These analyses agree with experimental observations.
- Mechanistic or non-mechanistic predictive equations can reliably predict the yield rotation. Although both methods lead to similar results, recommendations are as follows: the former is preferred for generalization, except when the plate yields first in tension. The latter equation may be used in such cases since the mechanics-based equation cannot appropriately describe this failure mode, including the base plate's membrane action.
- The referred connections' yield and ultimate strength parameters can be accurately predicted with the well-known mechanistic equations from Design Guide 1 of the American Institute of Steel Construction. These parameters coincide with the minor and significant moments between those corresponding to the plate yielding in compression/tension and anchor rods in tension, respectively.
- The predictive equations proposed in this work can accurately predict the full-range monotonic backbone M-θ curves of exposed column-base plates, following a trilinear model.
- The median values of the tested and predicted yield rotations of 63 specimens are equal to 0.6 % and 0.7 %, respectively. Therefore, exposed column-base plates in MRF buildings are expected to deform inelastically even under inter-story-drifts lower than 1 %, commonly associated with system-level yielding.
- The multivariable regression analysis performed in this study shows that axial loads have a primary role in predicting the strength and rotational parameters of exposed column-base plates and, therefore, in their seismic performance.

Some remarks are provided for the proposed predictive equations. In the case of non-mechanistic equations, the confidence level of the models is higher when the input data is within the range of experimental data – and extrapolation might result in a loss of accuracy. In addition, as most of the specimens in the set of data are code-designed ones, the proposed regression equations are mainly applicable to exposed column-base plate configurations, which are fairly regular in configuration (e.g., AISC Design Guide 1 [12] and Eurocode 3:1–8 [40]). Apart from this analysis, some conditions do not apply to the proposed equations (both regression- and mechanics-based), like connections in biaxial bending and those with highly pretensioned anchor rods; Hassan et al. [59] and Fasaee et al. [8] provides details for capacity characterization in the former case, while Trautner et al. [19] in the latter. Despite these apparent limitations, the methods presented in this paper are also expected to provide robust and accurate predictions for out-of-sample data, as shown by the results of the cross-validation tests performed in this study. Furthermore, it is essential to note that the models developed herein are only for the monotonic backbone. Simulation of a complete cyclic response will require estimating additional parameters that control deterioration and other effects; Torres-Rodas et al. [33] provide some guidance. Notwithstanding these limitations, the approaches and accompanying web tools are expected to significantly facilitate the simulation of ECBP connections in nonlinear structural analysis.

CRediT authorship contribution statement

Sergio Villar-Salinas: Writing – review & editing, Writing – original draft, Visualization, Software, Resources, Project administration, Methodology, Investigation, Funding acquisition, Formal analysis, Data curation, Conceptualization. **Amit Kanvinde:** Writing – review & editing, Visualization, Supervision, Methodology, Formal analysis, Conceptualization. **Francisco López-Almansa:** Validation, Supervision.

Declaration of competing interest

The authors declare that they have no known competing financial interests or personal relationships that could have appeared to influence the work reported in this paper.

Data availability

We have shared the link to our data in the text of the manuscript

Acknowledgments

The first author greatly appreciates the financial support from Fundación Carolina and Universidad Tecnológica de Bolívar during his

PhD research. Diana Carrasquilla and Cristian González's contribution to the development and implementation of the web-based interactive tools is thankfully acknowledged. Sebastian Pacheco's help with digitalizing moment-rotation curves is greatly appreciated. The authors recognize each filiation institution for facilitating or financing research activities.

References

[1] I. Piana, A.F.G. Calenzani, Study of design methodologies of steel column bases, Ibracon Struct. Mater. J. 11 (2018) 203–243, https://doi.org/10.1590/s1983-41952018000100011.
[2] Eröz Murat, White Donald W., DesRoches Reginald, Direct analysis and design of steel frames accounting for partially restrained column base conditions, J. Struct. Eng. 134 (2008) 1508–1517, https://doi.org/10.1061/(ASCE)0733-9445(2008)134:9(1508.
[3] J.P. Jaspart, D. Vandegans, Application of the component method to column bases, J. Constr. Steel Res. 48 (1998) 89–106, https://doi.org/10.1016/S0143-974X(98)90196-1.
[4] J.C. Ermopoulos, G.T. Michaltsos, Analytical modelling of stress distribution under column base plates, Second World Conf. Steel Constr. 46 (1998) 246, https://doi.org/10.1016/S0143-974X(98)80026-6.
[5] J.E. Grauvilardell, D. Lee, J.F. Hajjar, R.J. Dexter, Synthesis of design, testing and analysis research on steel column base plate connections in high-seismic zones 181, 2005.
[6] K. Tsavdaridis, M. Shaheen, C. Baniotopoulos, E. Salem, Analytical approach of anchor rod stiffness and Steel Base-plate calculation under tension, Structures 5 (2015) 207–218, https://doi.org/10.1016/j.istruc.2015.11.001.
[7] S. Khodaie, M.R. Mohamadi-shooreh, M. Mofid, Parametric analyses on the initial stiffness of the SHS column base plate connections using FEM, Eng. Struct. 34 (2012) 363–370, https://doi.org/10.1016/j.engstruct.2011.09.026.
[8] M.A.K. Fasaee, M.R. Banan, S. Ghazizadeh, Capacity of exposed column base connections subjected to uniaxial and biaxial bending moments, J. Constr. Steel Res. 148 (2018) 361–370, https://doi.org/10.1016/j.jcsr.2018.05.025.
[9] F. Zareian, A. Kanvinde, Effect of column-base flexibility on the seismic response and safety of steel moment-resisting frames, Earthquake Spectra 29 (2013) 1537–1559, https://doi.org/10.1193/030512EQS062M.
[10] M. Latour, G. Rizzano, Mechanical modelling of exposed column base plate joints under cyclic loads, J. Constr. Steel Res. 162 (2019) 105726, https://doi.org/10.1016/j.jcsr.2019.105726.
[11] A.M. Kanvinde, S.J. Jordan, R.J. Cooke, Exposed column base plate connections in moment frames — simulations and behavioral insights, J. Constr. Steel Res. 84 (2013) 82–93, https://doi.org/10.1016/j.jcsr.2013.02.015.
[12] J.M. Fisher, L.A. Kloiber, Design Guide 1: Base Plate and Anchor Rod Design, second edition, 2006. https://www.aisc.org/Design-Guide-1-Base-Plate-and-Anchor-Rod-Design-Second-Edition-Print#.XVfizOhKhPY.
[13] AISC 341, Seismic Provisions for Structural Steel Buildings. https://www.aisc.org/globalassets/aisc/publications/standards/seismic-provisions-for-structural-steel-buildings-ansi-aisc-341-16.pdf, 2022. (Accessed 12 November 2018).
[14] A. Kanvinde, D. Grilli, F. Zareian, Rotational stiffness of exposed column base connections: experiments and analytical models, J. Struct. Eng. 138 (2012) 549–560, https://doi.org/10.1061/(ASCE)ST.1943-541X.0000495.
[15] M. Latour, V. Piluso, G. Rizzano, Rotational behaviour of column base plate connections: experimental analysis and modelling, Eng. Struct. 68 (2014) 14–23, https://doi.org/10.1016/j.engstruct.2014.02.037.
[16] I. Gomez, A. Kanvinde, C. Smith, Exposed Column Base Connections Subjected to Axial Compression and Flexure, American Institute of Steel Construction, AISC, Chicago, IL USA, 2010.
[17] T. Falborski, A.S. Hassan, A.M. Kanvinde, Column base fixity in steel moment frames: observations from instrumented buildings, J. Constr. Steel Res. 168 (2020) 105993, https://doi.org/10.1016/j.jcsr.2020.105993.
[18] A.S. Hassan, B. Song, C. Galasso, A. Kanvinde, Seismic Performance of Exposed Column–Base Plate Connections with Ductile Anchor Rods, J. Struct. Eng. 148 (2022) 04022028, https://doi.org/10.1061/(ASCE)ST.1943-541X.0003298.
[19] C.A. Trautner, T. Hutchinson, P.R. Grosser, J.F. Silva, Investigation of steel column–baseplate connection details incorporating ductile anchors, J. Struct. Eng. 143 (2017) 04017074, https://doi.org/10.1061/(ASCE)ST.1943-541X.0001759.
[20] A. Picard, D. Beaulieu, Behaviour of a simple column base connection, Can. J. Civ. Eng. 12 (1985) 126–136, https://doi.org/10.1139/l85-013.
[21] R.E. Melchers, Column-base response under applied moment, J. Constr. Steel Res. 23 (1992) 127–143, https://doi.org/10.1016/0143-974X(92)90040-L.
[22] K.K. Hon, R.E. Melchers, Experimental behaviour of steel column bases, J. Constr. Steel Res. 9 (1988) 35–50, https://doi.org/10.1016/0143-974X(88)90055-7.
[23] F. Kavoura, B. Gencturk, M. Dawood, Evaluation of Existing Provisions for Design of "Pinned" Column Base-Plate Connections, 2018, https://doi.org/10.1016/j.jcsr.2018.05.030.
[24] F. Kavoura, B. Gencturk, M. Dawood, M. Gurbuz, Influence of base-plate connection stiffness on the design of low-rise metal buildings, J. Constr. Steel Res. 115 (2015) 169–178, https://doi.org/10.1016/j.jcsr.2015.08.005.
[25] F. Kavoura, B. Gencturk, M. Dawood, Reversed cyclic behavior of column-to-foundation connections in low-rise metal buildings, J. Struct. Eng. 143 (2017) 04017095, https://doi.org/10.1061/(ASCE)ST.1943-541X.0001821.
[26] C.G. Salmon, L. Schenker, B.G. Johnston, Moment-rotation characteristics of column anchorages, Trans. Am. Soc. Civ. Eng. 122 (1957) 132–154, https://doi.org/10.1061/TACEAT.0007496.
[27] J.Ch. Ermopoulos, G.N. Stamatopoulos, Mathematical modelling of column base plate connections, J. Constr. Steel Res. 36 (1996) 79–100, https://doi.org/10.1016/0143-974X(95)00011-J.
[28] R.M. Drake, S.J. Elkin, Beam-column base plate design-LRFD method, Engl. J. 36 (1999) 16–38.
[29] A.M. Kanvinde, P. Higgins, R.J. Cooke, J. Perez, J. Higgins, Column base connections for hollow steel sections: seismic performance and strength models, J. Struct. Eng. 141 (2015) 04014171, https://doi.org/10.1061/(ASCE)ST.1943-541X.0001136.
[30] M. Dumas, D. Beaulieu, A. Picard, Characterization equations for steel column base connections, Can. J. Civ. Eng. 33 (2006) 409–420, https://doi.org/10.1139/l05-054.
[31] H. Díaz, E. Nuñez, C. Oyarzo-Vera, Monotonic response of exposed base plates of columns: numerical study and a new design method, Metals 220 (2020) 396, https://doi.org/10.3390/met10030396.
[32] M. Latour, G. Rizzano, A theoretical model for predicting the rotational capacity of steel base joints, J. Constr. Steel Res. 91 (2013) 89–99, https://doi.org/10.1016/j.jcsr.2013.08.009.
[33] P. Torres Rodas, Z. Farzin, K. Amit, Hysteretic model for exposed column–base connections, J. Struct. Eng. 142 (2016) 04016137, https://doi.org/10.1061/(ASCE)ST.1943-541X.0001602.
[34] G.N. Stamatopoulos, J.Ch. Ermopoulos, Experimental and analytical investigation of steel column bases, J. Constr. Steel Res. 67 (2011) 1341–1357, https://doi.org/10.1016/j.jcsr.2011.03.007.
[35] G. Abdollahzadeh, M. Ghobadi, Mathematical modeling of column-base connections under monotonic loading, Civ. Eng. Infrastruct. J. 47 (2014) 255–272, https://doi.org/10.7508/ceij.2014.02.008.
[36] A. Mohabeddine, Y.W. Koudri, J.A.F.O. Correia, J.M. Castro, Rotation capacity of steel members for the seismic assessment of steel buildings, Eng. Struct. 244 (2021) 112760, https://doi.org/10.1016/j.engstruct.2021.112760.
[37] D.G. Lignos, H. Krawinkler, Deterioration modeling of steel components in support of collapse prediction of steel moment frames under earthquake loading, J. Struct. Eng. 137 (2011) 1291–1302, https://doi.org/10.1061/(ASCE)ST.1943-541X.0000376.
[38] Y.-C. You, D. Lee, Development of improved exposed column-base plate strong-axis joints of low-rise steel buildings, J. Constr. Steel Res. 169 (2020) 106062, https://doi.org/10.1016/j.jcsr.2020.106062.
[39] C.A. Trautner, T. Hutchinson, P.R. Grosser, J.F. Silva, Effects of detailing on the cyclic behavior of steel baseplate connections designed to promote anchor yielding, J. Struct. Eng. 142 (2016) 04015117, https://doi.org/10.1061/(ASCE)ST.1943-541X.0001361.
[40] CEN, Eurocode 3: Design of steel structures - Part 1–8: Design of joints (EN 1993-1-8 :2005), Brussels, European Comitee for Standarization, 2005.
[41] S. Demir, M. Husem, S. Pul, Failure analysis of steel column-RC base connections under lateral cyclic loading, Struct. Eng. Mech. 50 (2014) 459–469, https://doi.org/10.12989/sem.2014.50.4.459.
[42] J.-H. Choi, Y. Choi, An experimental study on inelastic behavior for exposed-type steel column bases under three-dimensional loadings, J. Mech. Sci. Technol. 27 (2013) 747–759, https://doi.org/10.1007/s12206-012-0901-x.
[43] M. Fahmy, B. Stojadinovic, S.C. Goel, Analytical and experimental studies on the seismic response of steel column bases, in: Vancouver, Canadá, 1999, pp. 245–250.
[44] J.J. Burda, A. Itani, Studies of Seismic Behavior of Steel Base Plates, CCEER 99-7,, Center for Civil Engineering Earthquake Research (CEER), Reno, Nevada, USA, 1999.
[45] A.T. Wheeler, M.J. Clarke, G.J. Hancock, T.M. Murray, Design model for bolted moment end plate connections joining rectangular hollow sections, J. Struct. Eng. 124 (1998) 164–173, https://doi.org/10.1061/(ASCE)0733-9445(1998)124:2(164).
[46] F. Wald, I. Simek, Z. Sokol, J. Seifer, The column-base stiffness tests, v semi-rigid behaviour of civil engineering structural connections, Proc. Second State Art Workshop, Brussels, 1994, pp. 273–282.
[47] D.P. Thambiratnam, P. Paramasivam, Base plates under axial loads and moments, J. Struct. Eng. 112 (1986) 1166–1181, https://doi.org/10.1061/(ASCE)0733-9445(1986)112:5(1166).
[48] S. Chatterjee, A.S. Hadi, Regression Analysis by Example, Wiley, Somerset, 2015. https://public.ebookcentral.proquest.com/choice/publicfullrecord.aspx?p=918623&entityid=urn:mace:eduserv.org.uk:athens:provider:liv.ac.uk (accessed March 9, 2022).
[49] M. Aladsani, H.V. Burton, S. Abdullah, J. Wallace, Explainable machine learning model for predicting drift capacity of reinforced concrete walls, ACI Struct. J. 119 (2022), https://doi.org/10.14359/51734484.
[50] H. Sun, H.V. Burton, H. Huang, Machine learning applications for building structural design and performance assessment: state-of-the-art review, J. Build. Eng. 33 (2021) 101816, https://doi.org/10.1016/j.jobe.2020.101816.
[51] T. Obuchi, Y. Kabashima, Cross validation in LASSO and its acceleration, J. Stat. Mech. Theory Exp. 2016 (2016) 053304, https://doi.org/10.1088/1742-5468/2016/05/053304.
[52] A.B. Kabir, A. Hasan, A.M. Billah, Failure mode identification of column base plate connection using data-driven machine learning techniques, Eng. Struct. 240 (2021) 112389, https://doi.org/10.1016/j.engstruct.2021.112389.
[53] D. Nettleton, Selection of Variables and Factor Derivation, Commer. Data Min., Elsevier, in, 2014, pp. 79–104, https://doi.org/10.1016/B978-0-12-416602-8.00006-6.

[54] Simple Linear Regression, in: Regres. Anal. Ex., John Wiley & Sons, Inc., Hoboken, NJ, USA, 2006, pp. 21–51, https://doi.org/10.1002/0470055464.ch2.
[55] D.K. Dalal, M.J. Zickar, Some common myths about centering predictor variables in moderated multiple Regression and polynomial Regression, Organ. Res. Methods 15 (2012) 339–362, https://doi.org/10.1177/1094428111430540.
[56] C.K. Ender, D. Tofighi, Centering predictor variables in cross-sectional multilevel models: a new look at an old issue, Psychol. Methods 12 (2007) 121–138, https://doi.org/10.1037/1082-989X.12.2.121.
[57] J.A.S.P. Team, JASP (Version 0.17.1) [Computer software], 2023.
[58] T.G. Wakjira, A. Abushanab, U. Ebead, W. Alnahhal, FAI: fast, accurate, and intelligent approach and prediction tool for flexural capacity of FRP-RC beams based on super-learner machine learning model, Mater. Today Commun. 33 (2022) 104461, https://doi.org/10.1016/j.mtcomm.2022.104461.
[59] A.S. Hassan, P. Torres-Rodas, L. Giulietti, A. Kanvinde, Strength characterization of exposed column base plates subjected to axial force and biaxial bending, Eng. Struct. 237 (2021) 112165, https://doi.org/10.1016/j.engstruct.2021.112165.